

## Numerical simulation of SnS/CZTSSe heterojunction solar cells

J. R. Yuan, J. S. Wang, S. Q. Liu, H. H. Zhao, P. Wang, X. H. Deng

*Department of Physics, Nanchang University, Nanchang 330031, China*

This work combines the advantages of SnS and CZTSSe to constitute the SnS/CZTSSe heterojunction solar cells, and the effects of various factors on cell performance were studied by using numerical simulation. The results show that the optimal thickness of CZTSSe and SnS are  $0.1\text{ }\mu\text{m}$  and  $2.0\text{ }\mu\text{m}$ , respectively. Furthermore, the optimal doping concentrations of CZTSSe and SnS are  $1\times 10^{17}\text{ cm}^{-3}$  and  $1\times 10^{16}\text{ cm}^{-3}$ , respectively. In addition, defect states have little impacts on the cell performance when the density of Gaussian defect states of CZTSSe and SnS are less than  $1\times 10^{16}\text{ cm}^{-3}$  and  $1\times 10^{14}\text{ cm}^{-3}$ , respectively, and the density of tail defect states of these two materials are both less than  $1\times 10^{19}\text{ cm}^{-3}\text{ eV}^{-1}$ . Moreover, the potential conversion efficiency of the SnS/CZTSSe heterojunction solar cells can reach 23.92%. Therefore, the SnS/CZTSSe heterojunction solar cell may be a promising photovoltaic structure.

(Received October 7, 2022; Accepted January 7, 2023)

**Keywords:** CZTSSe, SnS, Heterojunction, Simulation

### 1. Introduction

With the increasing environmental pollution and severe shortage of traditional fossil energy, solar photovoltaic power generation is increasingly valued due to the characteristics of cleaning, safety and sustainability. In particular, solar cells with simple structure, high efficiency and low cost have become an important development direction [1-5].

SnS is a brown IV-IV layer-shaped compound semiconductor material with orthorhombic structure, and it is generally p-type semiconductor. SnS possesses direct bandgap with 1.2-1.5 eV, which is close to the optimal bandgap of solar cells. SnS has a large optical absorption coefficient ( $\alpha > 10^4\text{ cm}^{-1}$ ) in the visible light region [6]. In addition, S and Sn elements are rich, low cost and little harm to the environment, and the preparation and production process of SnS are relatively simple. Thus, SnS thin film solar cell is a photovoltaic device with great application prospect [7-11]. CZTSSe is usually an n-type direct bandgap semiconductor material, whose bandgap is 1.2 eV [12-13]. Based on the physical properties of the above two materials, the SnS/CZTSSe heterojunction solar cell may be a promising structure.

Up to now, the conversion efficiency of SnS/CZTSSe heterojunction solar cells is still low [14-18], and the origin of low-efficiency is not clear. Therefore, the effects of material thickness, doping concentration, Gaussian defect state and band tail defect state on the performance

---

\* Corresponding author: yuanjiren@ncu.edu.cn

<https://doi.org/10.15251/JOR.2023.191.31>

of SnS/CZTSSe solar cells are studied by using numerical simulation. We hope to demonstrate the feasibility of SnS/CZTSSe solar cell structure, especially to prove that the SnS/CZTSSe solar cell has high potential photoelectric conversion efficiency, so as to provide theoretical guide for the actual preparation of this solar cell.

## 2. Physical model and simulation method

Figure 1 shows the structure of SnS/CZTSSe solar cell, in which CZTSSe is an n-type emitter layer, and SnS is p-type absorption layer. The top layer is indium tin oxide (ITO) material, and the substrate is Molybdenum (Mo) and conductive glass.

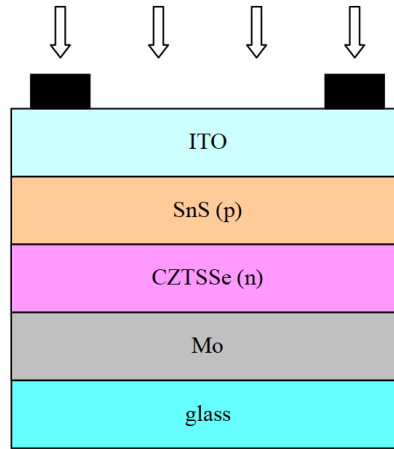


Fig. 1. Structure diagram of SnS/CZTSSe solar cell

In this work, the SnS/CZTSSe heterojunction solar cells are calculated and analyzed by using wxAMPS software [19], which was developed by Pennsylvania State University, University of Illinois at champagne and Nankai University. The main working process of semiconductor devices can be described by a set of semiconductor basic equations. Under certain boundary conditions, the ideal working characteristics of most semiconductor devices can be obtained by solving this set of equations. The three basic semiconductor equations and boundary conditions are as below:

$$\frac{d}{dx}(\varepsilon(x) \frac{d\psi}{dx}) = q(p(x) - n(x) + N_D^+(x) - N_A^-(x) + p_t(x) - n_t(x)) \quad (1)$$

$$\frac{dJ_n}{dx} = q(R(x) - G(x)) \quad (2)$$

$$\frac{dJ_p}{dx} = q(G(x) - R(x)) \quad (3)$$

Formula (1) is one-dimensional Poisson equation, and the other two formulas are electron and hole continuity equations, respectively. Where  $\varepsilon$  is the dielectric constant,  $\psi$  is the

electrostatic potential,  $q$  is the electric charge,  $n$  is the free electron concentration,  $p$  is the free hole concentration,  $n_t$  is the trapped electron concentration,  $p_t$  is the trapped hole concentration,  $N_D^+$  is the donor concentration and  $N_A^-$  is the acceptor concentration.  $J_n$  is the electron current density,  $J_p$  is the hole current density, while  $G$  is the photogenerated carrier generation rate, and  $R$  is the photogenerated carrier recombination rate,  $x$  is the cell thickness.

Boundary conditions are as below:

$$\psi(0) = \psi_0 - V \quad (4)$$

$$\psi(L) = 0 \quad (5)$$

$$J_p(0) = -qS_{p0}[p(0) - p_0(0)] \quad (6)$$

$$J_n(0) = qS_{n0}[n(0) - n_0(0)] \quad (7)$$

$$J_p(L) = qS_{pL}[p(L) - P_0(L)] \quad (8)$$

$$J_n(L) = -qS_{nL}[n(L) - n_0(L)] \quad (9)$$

Among them,  $\Psi_0$  is the built-in potential,  $V$  is the bias voltage,  $n_0$  is the electron concentration at the electrode interface, and  $p_0$  is the hole concentration at the electrode interface.  $S_{n0}$ ,  $S_{p0}$ ,  $S_{nL}$  and  $S_{pL}$  represent the surface recombination rate of electrons and holes at the front and rear electrode interfaces, respectively.

In terms of electrical properties, defect states can be divided into acceptor-type defects and donor-type defects. The distribution of defect states in the energy band can be divided into exponential distribution, Gaussian distribution and uniform distribution. In wxAMPS, the exponential distribution model is often used to explain the band tail structure formed by defects in crystals. Figure 2 shows the distribution of band tail defect states. The relationship between band tail defect state density and energy is as follows:

$$g_a(E) = G_{DO} \cdot \exp\left(\frac{E_V - E}{E_D}\right) \quad (10)$$

$$g_d(E) = G_{AO} \cdot \exp\left(\frac{E - E_C}{E_A}\right) \quad (11)$$

Among them,  $g_a$  is acceptor-type band tail defect state,  $g_d$  is donor-type band tail defect state,  $G_{AO}$  is conduction band bottom energy density,  $G_{DO}$  is valence band top energy density,  $E_C$  is conduction band edge,  $E_V$  is valence band edge,  $E_A$  is conduction band tail

characteristic energy level, and  $E_D$  is valence band tail characteristic energy level.

Another defect state mode Gaussian defect state is also provided in wxAMPS, and the defect state presents a Gaussian distribution trend in the energy band. The Gaussian defect state is suitable for the distribution of most materials in the energy band. Figure 3 shows the distribution of Gaussian states. The relationship between Gaussian defect state distribution and energy in the material can be expressed as follows:

$$G_A(E) = N_{AG} \cdot \exp\left[-\frac{1}{2}\left(\frac{E - E_{ACP}}{W_{DSA}}\right)^2\right] \quad (12)$$

$$G_D(E) = N_{DG} \cdot \exp\left[-\frac{1}{2}\left(\frac{E - E_{DON}}{W_{DSD}}\right)^2\right] \quad (13)$$

Among them,  $G_A(E)$  is acceptor-type Gaussian defect state,  $G_D(E)$  is donor-type Gaussian defect state,  $N_{AG}$  is Gaussian like acceptor distribution density,  $N_{DG}$  is Gaussian like donor state density,  $E_{ACP}$  is acceptor-type peak energy level,  $E_{DON}$  is donor-type peak energy level,  $W_{DSA}$  is acceptor-type split energy level width, and  $W_{DSD}$  is donor type split energy level width.

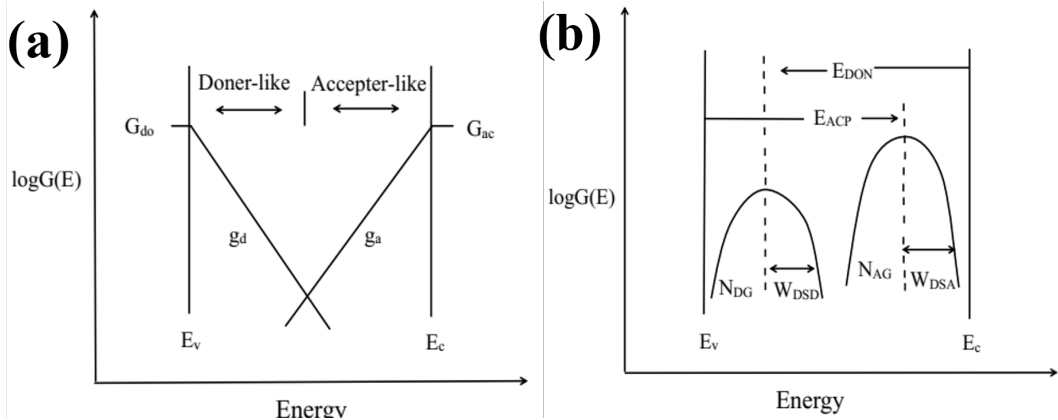


Fig. 2. (a) Distribution diagram of band tail defects, (b) Schematic diagram of Gaussian defect state distribution.

Gaussian defect states and band tail defect states describe the distribution of two different defects. Gaussian defect states are mainly caused by dangling bonds, while band tail defect states are caused mainly by localized states which formed by aperiodic lattice.

During the simulation calculation, AM1.5 standard spectrum is used as the incident light source. The temperature is 300 K. The reflectivity of the incident light on the front and rear surfaces is 0 and 1, respectively. Some parameters used in the simulation calculation are shown in Table 1 [20-22].

Table 1. Main material parameters of SnS/CZTSSe solar cells.

Material parameters /units	CZTSSe(n)	SnS(p)
Thickness/nm	Variable	Variable
Dielectric constant/ $\epsilon$	13	13
Band gap/eV	1.2	1.35
Electron affinity/eV	4.1	4
Effective conduction band density/cm <sup>-3</sup>	$7.5 \times 10^{17}$	$1.18 \times 10^{18}$
Effective valence band density/cm <sup>-3</sup>	$1.0 \times 10^{19}$	$2.24 \times 10^{18}$
Electron mobility/cm <sup>2</sup> .V <sup>-1</sup> s <sup>-1</sup>	100	20
Hole mobility/cm <sup>2</sup> .V <sup>-1</sup> s <sup>-1</sup>	0.25	100
Acceptor doping concentration/cm <sup>-3</sup>	0	Variable
Donor doping concentration/cm <sup>-3</sup>	Variable	0
Density of Gaussian states/cm <sup>-3</sup>	$1 \times 10^{15}$	$1 \times 10^{15}$
Donor and acceptor Gaussian/eV	1.12, 1.02	0.6, 0.7
Half height width of Gaussian /eV	0.10	0.05
Electron capture cross-sectional area of Gaussian defect state /cm <sup>2</sup>	$1 \times 10^{-15}$	$1 \times 10^{-14}$
Hole capture cross-sectional area of Gaussian defect state/cm <sup>2</sup>	$1 \times 10^{-14}$	$1 \times 10^{-15}$
Density of tail states/cm <sup>-3</sup> eV <sup>-1</sup>	$1 \times 10^{14}$	$1 \times 10^{14}$
Donor and acceptor characteristic energy levels/eV	0.05,003	0.01,0.01
Electron capture cross-sectional area of tail defect state/cm <sup>2</sup>	$1 \times 10^{-15}$	$1 \times 10^{-17}$
Hole capture cross-sectional area of tail defect state /cm <sup>2</sup>	$1 \times 10^{-17}$	$1 \times 10^{-15}$

### 3. Results and discussion

#### 3.1. Effect of SnS and CZTSSe thicknesses

Figure 3(a) shows the effect of SnS thickness on the performance of SnS/CZTSSe solar cells. It is found that the open-circuit voltage ( $V_{oc}$ ) gradually increases with the increase of SnS thickness. The short-circuit current density ( $J_{sc}$ ) increases from 18 mA/cm<sup>2</sup> to 33 mA/cm<sup>2</sup> when the SnS thickness increases from 0.1  $\mu$ m to 0.6  $\mu$ m. But with the continuous increase of thickness,  $J_{sc}$  changes little. Moreover, the filling factor (FF) increases with the increase of SnS thickness, and then gradually tends to be constant. The conversion efficiency ( $E_{ff}$ ) of the solar cell increases as the SnS thickness increases, and  $E_{ff}$  reaches the highest value when the SnS thickness is 2  $\mu$ m. Figure 3(b) shows the effect of CZTSSe thickness on the performance of the SnS/CZTSSe solar cells. When the thickness of CZTSSe is 0.1-1  $\mu$ m, the  $V_{oc}$ ,  $J_{sc}$ , FF and  $E_{ff}$  of solar cells changes little.

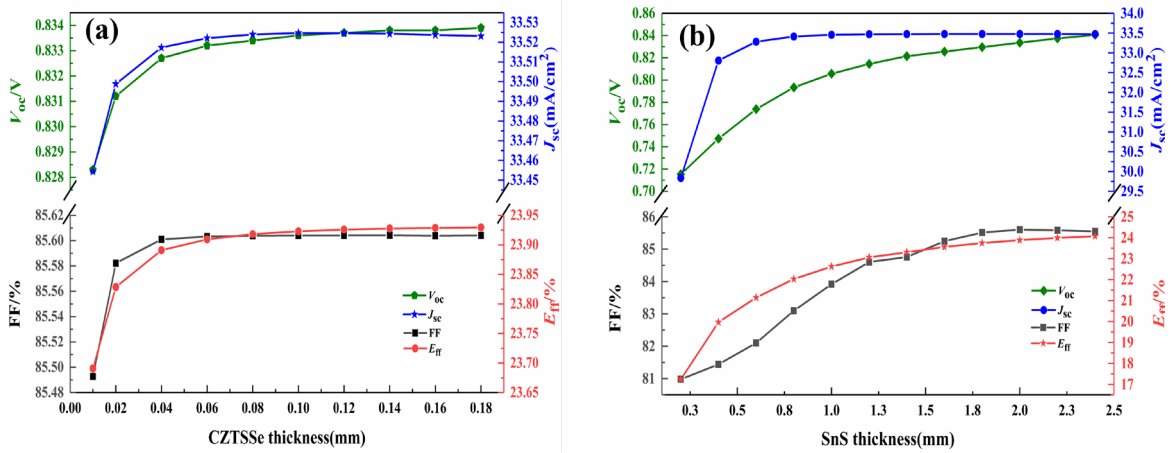


Fig. 3. Effects of SnS thickness and CZTSSe thickness on  $V_{oc}$ ,  $J_{sc}$ , FF and  $E_{ff}$

### 3.2. Effect of SnS and CZTSSe doping concentration

Figure 4(a) shows the effect of SnS doping concentration on  $V_{oc}$ ,  $J_{sc}$ , FF and  $E_{ff}$ . It can be seen that the  $V_{oc}$  and  $E_{ff}$  increase with the increase of SnS doping concentration. The doping concentration exceeds  $1 \times 10^{17} \text{ cm}^{-3}$ , the  $V_{oc}$  does not increase, but the conversion efficiency decreases slightly. When the SnS doping concentration exceeds  $1 \times 10^{15} \text{ cm}^{-3}$ , the  $J_{sc}$  decreases with its increase, and the FF increases steadily with the increase of doping concentration. So, considering various reference factors, the best doping concentration of SnS is  $1 \times 10^{16} \text{ cm}^{-3}$ .

Figure 4(b) shows the effect of CZTSSe doping concentration on the performance of the SnS/CZTSSe solar cells. It can be seen from the figure that the  $V_{oc}$ , FF and  $E_{ff}$  increase with the increase of doping concentration which increases from  $1 \times 10^{13} \text{ cm}^{-3}$  to  $1 \times 10^{17} \text{ cm}^{-3}$ . When the doping concentration exceeds  $1 \times 10^{17} \text{ cm}^{-3}$ , the curves of  $V_{oc}$ , FF and  $E_{ff}$  hardly changed. As can be seen from Fig. 5, with the increase of CZTSSe doping concentration, the overall electric field strength in the solar cell also increases. And the doping concentration is  $1 \times 10^{21} \text{ cm}^{-3}$ , the electric field strength of solar cell can reach  $1 \times 10^6 \text{ V/cm}$ . The results show that the solar cell has the best performance while the doping concentration of CZTSSe is set to  $1 \times 10^{17} \text{ cm}^{-3}$ .

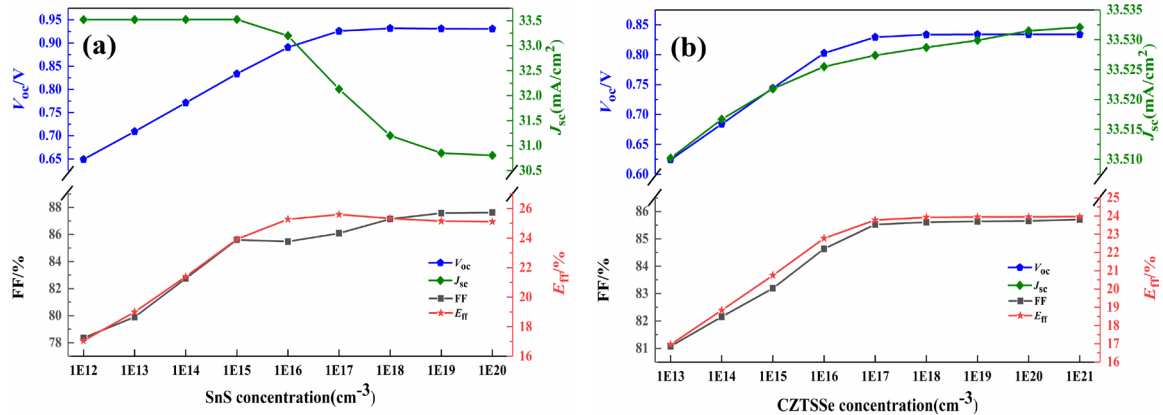


Fig. 4. Effects of SnS doping concentration and CZTSSe doping concentration on  $V_{oc}$ ,  $J_{sc}$ , FF and  $E_{ff}$

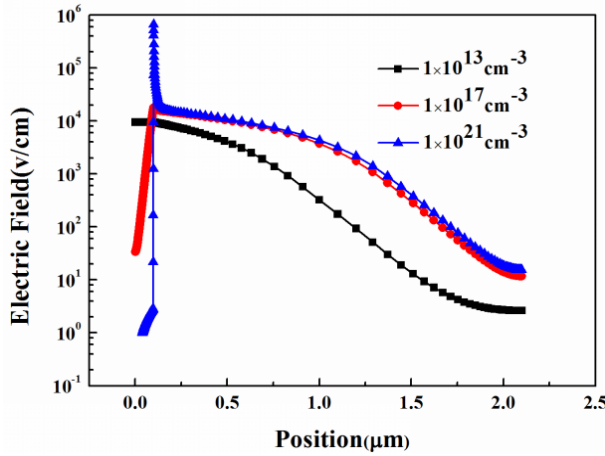


Fig. 5. Effects of CZTSSe doping concentration affecting electric field intensity

### 3.3. Effect of SnS and CZTSSe Gaussian defect states

As can be seen from Fig. 6(a), when the Gaussian defect state density is less than  $1 \times 10^{14} \text{ cm}^{-3}$ , SnS Gaussian defect states would not affect the performance of solar cells, and the overall performance of solar cells basically unchanged. While SnS Gaussian defect state density is greater than  $1 \times 10^{14} \text{ cm}^{-3}$ , each curve of solar cell decreases rapidly. As show in Fig. 6(b), when the density of CZTSSe Gaussian defect state is greater than  $1 \times 10^{17} \text{ cm}^{-3}$ , the  $V_{oc}$ ,  $J_{sc}$ , FF and  $E_{ff}$  decrease rapidly, and the performance curve changes obviously. The  $V_{oc}$  is reduced from 0.825 V to 0.720 V, the  $E_{ff}$  is reduced from 22.8% to 18%, and the performance is seriously degraded. Therefore, CZTSSe Gaussian defect state density should be less than  $1 \times 10^{16} \text{ cm}^{-3}$ .

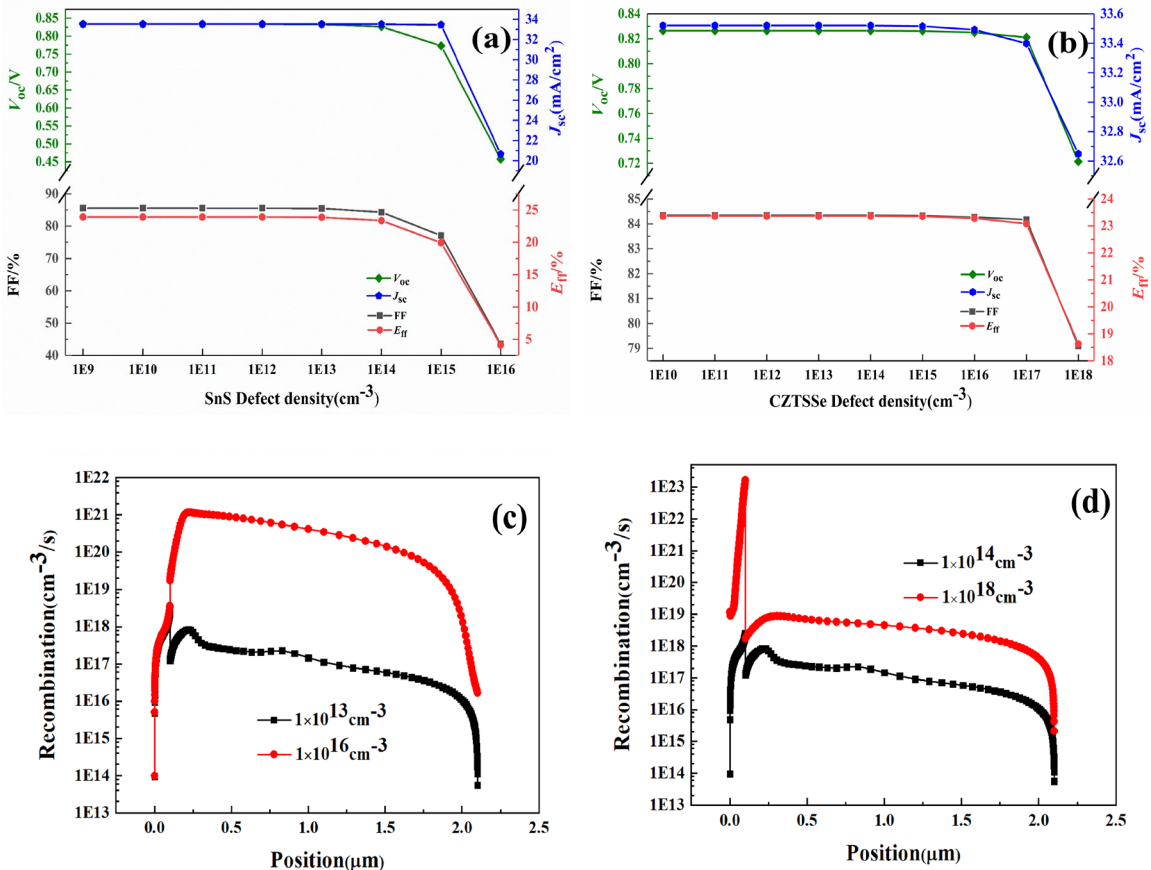


Fig. 6. Effects of SnS Gaussian defect states and CZTSSe Gaussian defect state on  $V_{oc}$ ,  $J_{sc}$ , FF,  $E_{ff}$  and recombination rate.

It can be seen from Fig. 6(c), when the density of Gaussian defect states in SnS increase, the recombination rate of carriers also increases obviously. The increase of density of Gaussian defect state leads to massive recombination of carriers, which deteriorates the performance of solar cells. Figure 6(d) shows the influence of CZTSSe Gaussian defect state on carrier recombination rate. It is observed that the recombination rate with the density of Gaussian defect states  $1 \times 10^{18} \text{ cm}^{-3}$  is much higher than that with the density of Gaussian defect states  $1 \times 10^{14} \text{ cm}^{-3}$ . Moreover, the recombination of photogenerated carriers is very obvious, and the recombination mainly occurs at the interface. The recombination seriously affects the performance of solar cells.

### 3.4. Effect of SnS and CZTSSe band tail defect states

Figure 7(a) shows the effect of SnS band tail defect state on the performance of solar cells. It can be seen that the density of band tail defect state in SnS is less than  $1 \times 10^{19} \text{ cm}^{-3} \text{ eV}^{-1}$ , the overall performance of solar cells is relatively stable. When it exceeds  $1 \times 10^{19} \text{ cm}^{-3} \text{ eV}^{-1}$ , the performance of solar cells decreased sharply. Therefore, the density of state of SnS band tail defect should be controlled to be less than  $1 \times 10^{19} \text{ cm}^{-3} \text{ eV}^{-1}$  so that the solar cell will possess good performance. Figure 7(b) shows the influence of CZTSSe band tail states on the performance of the SnS/CZTSSe solar cell. When the density of defect states at band tail is less than  $1 \times 10^{19} \text{ cm}^{-3} \text{ eV}^{-1}$ , the band tail defect states have little effect on the  $V_{oc}$ ,  $J_{sc}$ , FF and  $E_{ff}$  of the solar cells, and the performance curve have no change. While the defect state density exceeds  $1 \times 10^{19} \text{ cm}^{-3} \text{ eV}^{-1}$ , the overall performance of solar cells decreased rapidly. The results show that the density of CZTSSe band tail defect state should be less than  $1 \times 10^{19} \text{ cm}^{-3} \text{ eV}^{-1}$  so that the solar cell will obtain good performance.

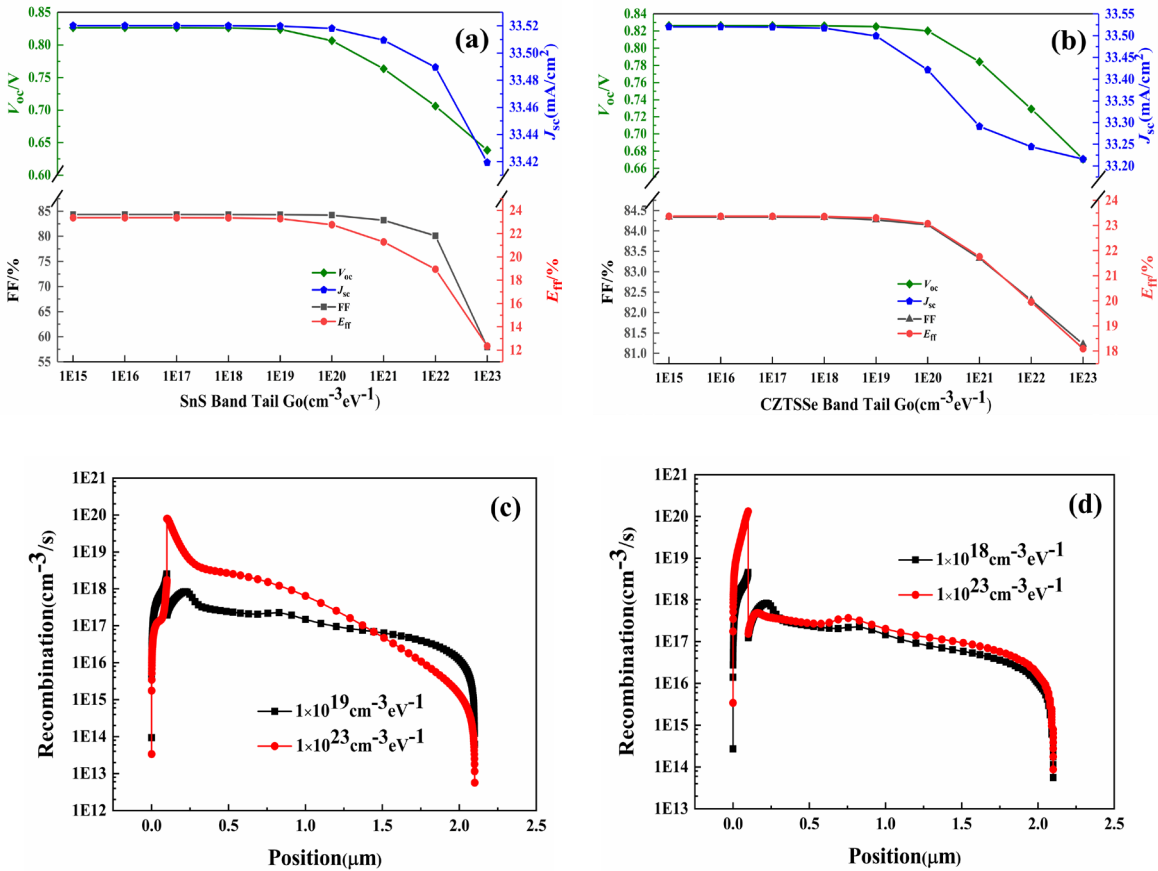


Fig. 7. Effects of SnS band tail defect state and CZTSSe band tail defect state on  $V_{oc}$ ,  $J_{sc}$ , FF,  $E_{ff}$  and carrier recombination rate.

As shown in Fig. 7(c), the increase of density of SnS band tail defect state will also increase the carrier recombination rate. The density of SnS band tail defect state increases from  $1 \times 10^{19} \text{ cm}^{-3} \text{ eV}^{-1}$  to  $1 \times 10^{23} \text{ cm}^{-3} \text{ eV}^{-1}$ , the recombination rate increase greatly. The increase of defect density can result in a large number of carrier recombination, deteriorating the performance of the solar cell. Fig. 7(d) shows that with the increase of CZTSSe band tail defect state density, the recombination rate of carriers at the interface increases rapidly, and the recombination rates at other positions change little. The interfacial recombination rate with the band tail defect state density  $1 \times 10^{23} \text{ cm}^{-3} \text{ eV}^{-1}$  is much higher than that with the band tail defect state density  $1 \times 10^{18} \text{ cm}^{-3} \text{ eV}^{-1}$ . It can be found that the CZTSSe band tail defect states have a great impacts on the carrier recombination at the interface.

### 3.5 Optimal I-V curve of SnS/CZTSSe solar cell

Through a series of optimal calculations, the potential photovoltaic parameters of the SnS/CZTSSe solar cell are as following: the  $V_{oc}$  of 0.83 V, the  $J_{sc}$  of  $33.52 \text{ mA/cm}^2$ , the  $FF$  of 85.60%, and the  $E_{ff}$  of 23.92%. The optimal I-V curve of SnS/CZTSSe solar cell is shown as Fig. 8.

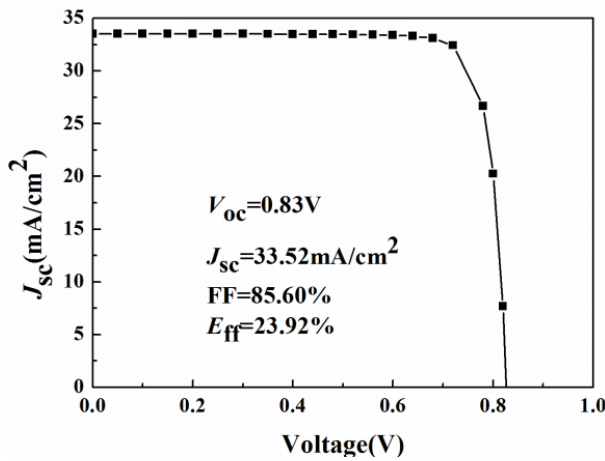


Fig. 8. Optimal I-V curve of CZTSSe/SnS solar cell

## 4. Conclusion

According to the physical properties of CZTSSe and SnS, SnS/CZTSSe solar cells are designed. The influencing of material thickness, doping concentration, Gaussian defect state and band tail defect state on the performance of the SnS/CZTSSe solar cell are studied. It is found that the optimal thicknesses of CZTSSe and SnS are  $0.1 \mu\text{m}$  and  $2.0 \mu\text{m}$ , respectively, and the optimal doping concentrations of CZTSSe and SnS are  $1 \times 10^{17} \text{ cm}^{-3}$  and  $1 \times 10^{16} \text{ cm}^{-3}$ , respectively. In order to obtain a good device performance, the density of Gaussian defect states of CZTSSe and SnS should be controlled to be less than  $1 \times 10^{16} \text{ cm}^{-3}$  and  $1 \times 10^{14} \text{ cm}^{-3}$ , respectively. The density of tail defect states of CZTSSe and SnS should be both less than  $1 \times 10^{19} \text{ cm}^{-3} \text{ eV}^{-1}$ . The potential cell performance is the  $V_{oc}$  of 0.83 V, the  $J_{sc}$  of  $33.52 \text{ mA/cm}^2$ , the  $FF$  of 85.6%, and the  $E_{ff}$  of 23.92%. These results indicate that SnS/CZTSSe heterojunction solar cell is a very promising high-efficiency photovoltaic device.

## Acknowledgements

This work was supported by the National Natural Science Foundation of China (No. 11964018). The authors acknowledge the free use of the wxAMPS program developed by Dr. Fonash's group at Pennsylvania State University and Dr. Yiming Liu at Nankai University & University of Illinois at champagne.

## References

- [1] Q. Jiang, Y. Zhao, X. Zhang, X. Yang, Y. Chen, Z. Chu, Q. Ye, X. Li, Z. Yin, J. You, *Nat. Photonics* 13, 460 (2019); <https://doi.org/10.1038/s41566-019-0398-2>
- [2] X. Zheng, Y. Hou, C. Bao, J. Yin, O. M. Bakr, *Nat. Energy* 5, 1 (2020).
- [3] M. Kim, G. H. Kim, T. K. Lee, I. W. Choi, S. K. Dong, *Joule* 3, 2179 (2019); <https://doi.org/10.1016/j.joule.2019.06.014>
- [4] J. Shi, Y. Li, H. Wu, Y. Luo, D. Li, Q. Meng, *Sci. Bull.* 66, 536 (2021); <https://doi.org/10.1016/j.scib.2020.11.004>
- [5] J. Du, J. Duan, Y. Duan, Q. Tang, *Sci. Chin. Mater.* 64, 798 (2021); <https://doi.org/10.1007/s40843-020-1499-8>
- [6] Y. Takano, K. Oyaizu, *Mater. Lett.* 228, 414 (2018); <https://doi.org/10.1016/j.matlet.2018.06.073>
- [7] J.Y. Cho, S. Sinha, M. G. Gang, J. Heo, *J. Alloys Compd.* 796, 160 (2021); <https://doi.org/10.1016/j.jallcom.2019.05.035>
- [8] H. Yun, B. Park, C. C. Yong, J. Im, T. J. Shin, I. S. Sang, *Adv. Energy Mater.* 35, 190134 (2019).
- [9] A. Voznyi, V. Kosyak, Y. Yeromenko, J. Keller, A. Opanasyuk, *Thin Solid Films* 709, 138 (2020); <https://doi.org/10.1016/j.tsf.2020.138153>
- [10] K. O. Hara, K. Arimoto, J. Yamanaka, K. Nakagawa, *Thin Solid Films* 706, 138064 (2020); <https://doi.org/10.1016/j.tsf.2020.138064>
- [11] X. Huang, H. Woo, D. Lee, P. Wu, M. Song, W. C. Jin, *Catalysts* 11, 236 (2021); <https://doi.org/10.3390/catal11020236>
- [12] Y. Zhang, Y. Sun, *Chalcogenide Letters* 13, 397 (2016).
- [13] D. H. Son, S. H. Kim, S. Y. Kim, Y. I. Kim, D. H. Kim, *J. Mater. Chem. A* 7, 25279 (2019); <https://doi.org/10.1039/C9TA08310C>
- [14] X. Zhao, Y. Pan, C. Zuo, F. Zhang, Z. Huang, L. Jiang, Y. Lai, L. Ding, F. Liu, *Sci. Bull.* 66, 880 (2021); <https://doi.org/10.1016/j.scib.2020.12.030>
- [15] B. Duan, J. Shi, D. Li, Y. Luo, H. Wu, Q. Meng, *Sci. Chin. Mater.* 63, 2371 (2020); <https://doi.org/10.1007/s40843-020-1385-0>
- [16] L. Guo, J. Shi, Q. Yu, B. Duan, X. Hu, J. Zhou, J. Wu, Y. Li, D. Li, H. Wu, Y. Luo, Q. Meng, *Sci. Bull.* 65, 738 (2020); <https://doi.org/10.1016/j.scib.2020.01.005>
- [17] H. Luan, B. Yao, Y. Li, R. Liu, Z. Ding, Z. Zhang, H. Zhao, L. Zhang, *J. Alloys Compd.* 876, 160160 (2021); <https://doi.org/10.1016/j.jallcom.2021.160160>

- [18] S. B. Machiche, L. Dehimi, H. Bencherif, F Pezzimenti, Silicon 43, 1 (2021).
- [19] Y. Liu, Y. Sun, A. Rockett, Solar Energy Materials & Solar Cells 98, 124 (2012);  
<https://doi.org/10.1016/j.solmat.2011.10.010>
- [20] A. Hemmani, B. Merah, H. Khachab, Chalcogenide Letters, 19(4), 259 (2022);  
<https://doi.org/10.15251/CL.2022.194.259>
- [21] B. Yassine, B. Tahar, G. Fathi, Chalcogenide Letters 19(8), 503 (2022);  
<https://doi.org/10.15251/CL.2022.198.503>
- [22] H. Ullah, B. Marí, Superlattices and Microstructures 72, 148 (2014);  
<https://doi.org/10.1016/j.spmi.2014.03.042>